SUPPLEMENTARY INFORMATION

Covalent Inactivation of *Mycobacterium tuberculosis* Isocitrate Lyase by *cis*-2,3-Epoxy-Succinic Acid

AUTHORS: Truc Viet Pham,[1,3,#] Drake M. Mellott,[1,#] Zahra Moghadamchargari,[2] Kevin Chen,[1] Inna Krieger,[1] Arthur Laganowsky,[2] James C. Sacchettini,[1,2] and Thomas D. Meek[1,*]

[1]Department of Biochemistry and Biophysics, Texas A&M University, College Station, Texas 77843, United States.

[2]Department of Chemistry, Texas A&M University, College Station, Texas 77843, United States.

[3]Present address: Tango Therapeutics, 100 Binney Street, Cambridge, Massachusetts 02142, United States.

*Corresponding author at tdmeek@tamu.edu.

CONTENTS

SUPPLEMENTARY INFORMATION

Figures and Results

Double Inhibition Studies.

Inhibition of ICL1 by two inhibitors, one a glyoxylate analogue (glycolate or (*R*)-lactate), and the other a succinate analogue (maleate) was evaluated at a fixed concentration of 0.05 mM D-isocitrate at 2 nM enzyme. As previously determined, glycolate and (*R*)-lactate were competitive inhibitors of D-isocitrate, and therefore bind to free enzyme, while maleate is uncompetitive vs. D-isocitrate, and binds to the ICL1-glyoxylate complex. The data were plotted as $1/v$ vs. [glycolate/K_{is}] and $1/v$ vs. [(*R*)-lactate/K_{is}] at changing-fixed concentrations of maleate (0 – 0.5 mM) (Figure S1), and were fitted to both eq S4 and S5. Both plots were intersecting above the $1/v$-axis, indicative of synergistic binding of the two inhibitors. The apparent K_i and K_j values for glycolate (K_j = 10.2 ± 0.3 μM) and maleate (K_j = 151 ± 7 μM (eq S4); K_j = 230 ± 20 μM (eq S5)) were comparable to the respective K_{is} and K_{ii} values determined for these inhibitors as competitive and uncompetitive inhibitors, respectively. Fitting to eq S4 and S5 gave respective parameters of: (eq S4): r^2 = 0.9981, V_{max} = 21.4 ± 0.2 units, K_i = 10.2 ± 0.3 μM, K_j = 151 ± 7 μM, α = 0.37 ± 0.03 and (eq S5): r^2 = 0.9981, V_{max} = 21.4 ± 0.2 units, K_i = 10.2 ± 0.3 μM, K_j = 262 ± 12 μM, α = 0.37 ± 0.03. For *R*-lactate vs. glycolate, fitting to eq S4 and S5 gave respective parameters of (eq S4): r^2 = 0.9728, V_{max} = 13.2 ± 0.2 units, K_j = 230 ± 20 μM, α = 0.4 ± 0.1 and r^2 = 0.9728, V_{max} = 13.2 ± 0.2 units, K_j = 400 ± 40 μM, α = 0.22 ± 0.08. These results demonstrated that not only does maleate bind to the ICL1-Glx complex, but also to the ICL1-glycolate and ICL1-(*R*)-lactate complexes as represented by the $IJ/\alpha K_iK_j$ terms in the denominators of eq S4 and S5. A value of 1 for α signifies that there is no synergistic binding between the two inhibitors in the EIJ complex, but since both plots were characterized by respective α values of 0.37 ± 0.03 (maleate vs. glycolate) and 0.4 ± 0.1 (maleate vs. [(*R*)-lactate), it is evident that synergistic binding of the two sets of inhibitors is present. Discrimination of fitting between these two equations is negligible, although the value of K_j is better determined by fitting to eq S5 in both cases.

SUPPLEMENTARY INFORMATION

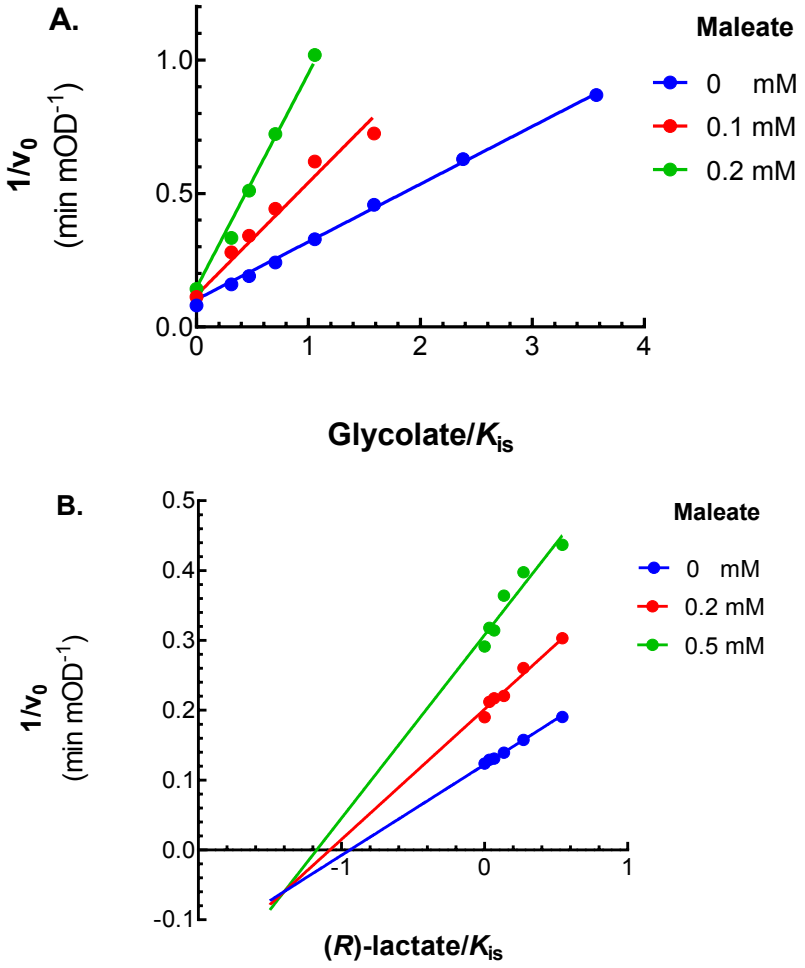

Figure S1. Yonetani-Theorell analysis of synergistic interactions (A) between glycolate and maleate, and (B) between maleate and (*R*)-lactate. The lines in the plot of maleate vs. glycolate apparently intersect on the 1/*v*-axis, while the lines in the plot of *R*-lactate vs. glycolate intersect below this axis. Qualitatively, this indicates significantly synergistic binding of glycolate with these two other inhibitors. When plotted against the ratio of the second inhibitor and its competitive inhibition constant we obtained: glycolate, K_{is} = 70 ± 6 µM; (*R*)-lactate, K_{is} = 2.3 ± 0.3 mM. Lines were drawn from linear regression analysis and the synergistic value α was calculated by equation α = -"x-axis intercept" x K_m/S which yielded α values of 0.36 ± 0.05 for the interaction between glycolate and maleate and 0.7 ± 0.1 for the interaction between (*R*)-lactate and maleate.

SUPPLEMENTARY INFORMATION

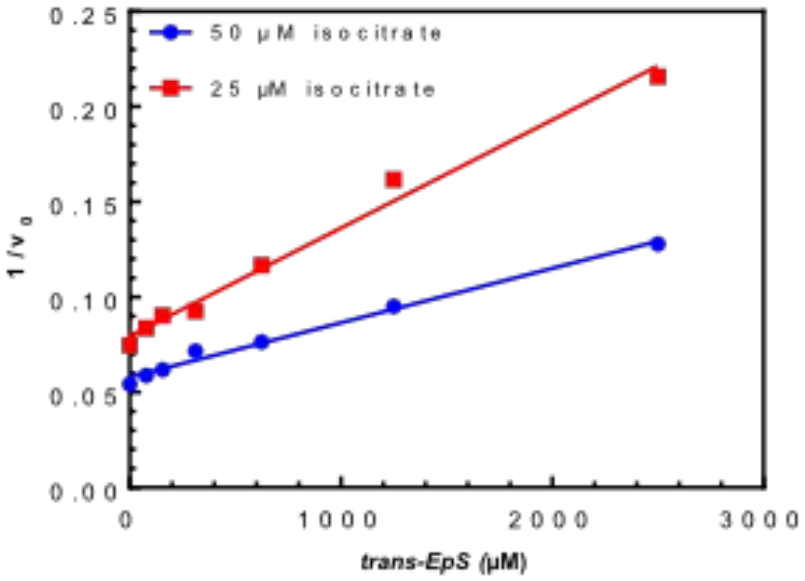

Figure S2. *Trans*-EpS inhibition is competitive vs. isocitrate. Dixon analysis was obtained by measuring initial velocity of ICL1 at 25 and 50 µM D-isocitrate and at 0-2500 µM *trans*-2,3-epoxysuccinate. The lines drawn through the data points were from fitting to $1/v_0 = K_{D\text{-}IC}[trans\text{-}EpS]/(V_{max}[D\text{-}isocitrate]K_i) + K_{D\text{-}IC}/(V_{max}[D\text{-}isocitrate])$ in which K_i is the apparent inhibition constant for a competitive inhibitor.

SUPPLEMENTARY INFORMATION

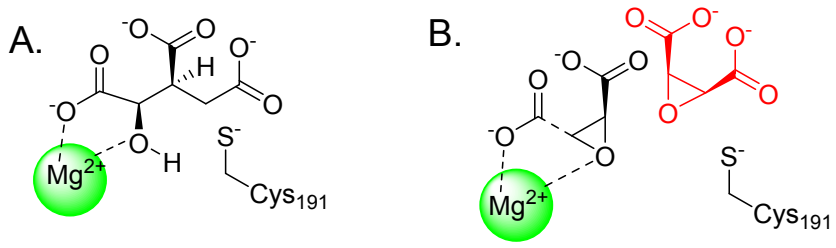

Figure S3. A. Scheme for proposed binding of (A) D-isocitrate in the active site of ICL1; B. binding of *trans*-EpS (black) versus *cis*-EpS (red) in the ICL1 active site.

SUPPLEMENTARY INFORMATION

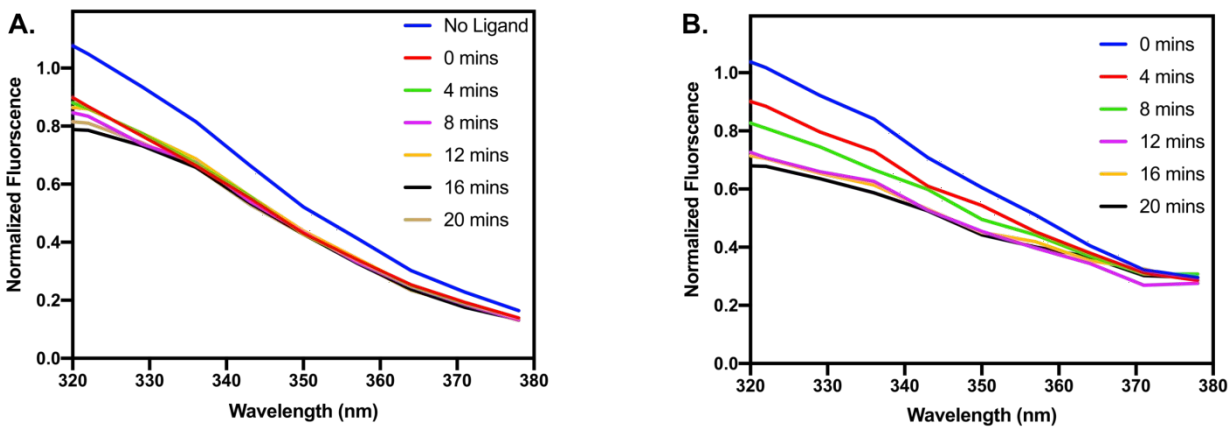

Figure S4. A. Fluorescent spectrum of 1 µM ICL1 in the presence of 100 µM glyoxylate normalized to 325 nm at varied time points. **B**. Deconvolution of the cis-EpS induced fluorescent change in the present of 100 µM glyoxylate, 1 µM *cis*-EpS and 1 µM ICL1. This spectrum was produced by subtraction of the glyoxylate alone spectrum, shown in **A**. from the original spectrum as seen in Fig. 2b, yielding the loss in fluorescence associated with *cis*-EpS inactivation of ICL1 alone in these multiple time point spectra.

SUPPLEMENTARY INFORMATION

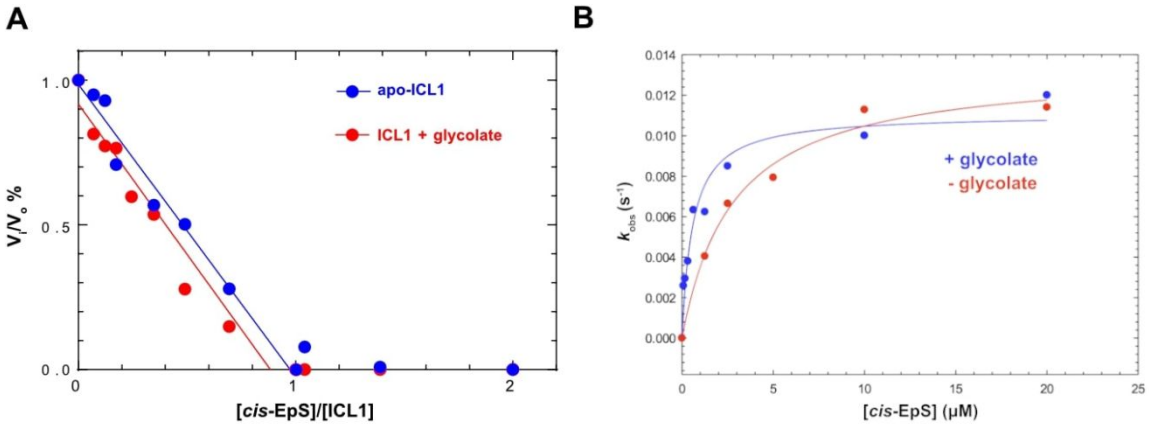

Figure S5. A. Stoichiometry of inactivation of ICL1 by *cis*-EpS in the presence or absence of glycolate. Residual enzymatic activity (V_i/V_0) of 0.5 μM ICL1 remaining after 24-hr pre-incubation with 0-1.0 μM *cis*-EpS, followed by 100-fold dilution of samples into a reaction mixture containing 1 mM D-isocitrate in order to ascertain the remaining enzymatic activity. Lines drawn through data points were from linear regression of data points in which [*cis*-EpS]/[ICL1] ≤ 1.0. **B** Concentration dependence of inactivation of ICL1 by *cis*-EpS in the presence and absence of glycolate. Following an initial 10-min pre-incubation, residual ICL1 activity was determined following 50-fold dilution of pre-incubated aliquots into reaction mixtures at 15-60 seconds intervals. Irreversible, time-dependent and saturable inactivation kinetics exhibited by *cis*-EpS was enhanced in the presence of 100 μM glycolate. Lines drawn through the data points were from fitting of data to eq 2. In the absence of glycolate, inactivation of free ICL1 by *cis*-EpS exhibited time-dependent irreversible kinetics (k_{inact} = (1.3 ± 0.08) x 10^{-3} sec^{-1} and K_{inact} = 2.8 ± 0.5 μM), whereas in the presence of glycolate (100 μM), k_{inact} = (1.1 ± 0.06) x 10^{-3} sec^{-1} and K_{inact} = 0.6 ± 0.1 μM. Note that these values of 6-fold and 5-fold higher, respectively, than k_{obs} values obtained for data in Figures 2a-c; data here were obtained at 37 ^{0} C, while those in Figure 3 at room temperature.

SUPPLEMENTARY INFORMATION

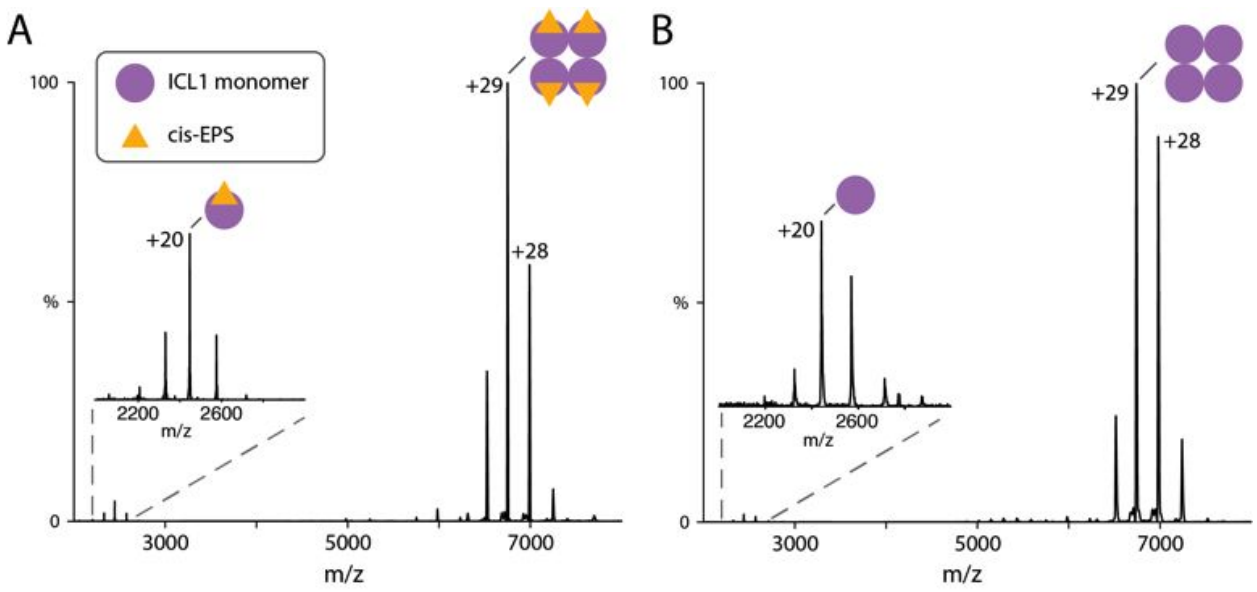

Figure S6. Nano-ESI-MS of tetrameric ICL1 obtained under activating energy conditions. The collision-induced dissociation spectra of (A) ICL1 in the presence of *cis*-EpS and (B) free ICL1. The mass spectra shown in **A** demonstrates that ICL1 is bound to *cis*-EpS. ICL1 was incubated with *cis*-EpS overnight, buffer exchanged into 200 mM ammonium acetate (pH 7.4), and then introduced into a Thermo Exactive Plus system with an extended mass-range Orbitrap mass spectrometer. The inset is the expansion of peaks at lower values of m/z which show ejected monomers. The theoretical and observed masses of free and *cis*-EpS-bound ICL1 are 48919.07 and 48918.32 (15.26 ppm) Da, respectively. **B**. The tetramer of ICL1 has a calculated mass of 195.148 Da, whereas the observed mass was 195,461.78 Da, indicating an addition of 77±17 Da (90.38 ppm) per monomer. When dissociated into monomers the observed mass was 48,787.94 Da, nearly equal to the calculated mass of an unmodified ICL1 monomer, 48,787.52 Da, suggesting that a non-covalent ligand is bound to the protein.

SUPPLEMENTARY INFORMATION

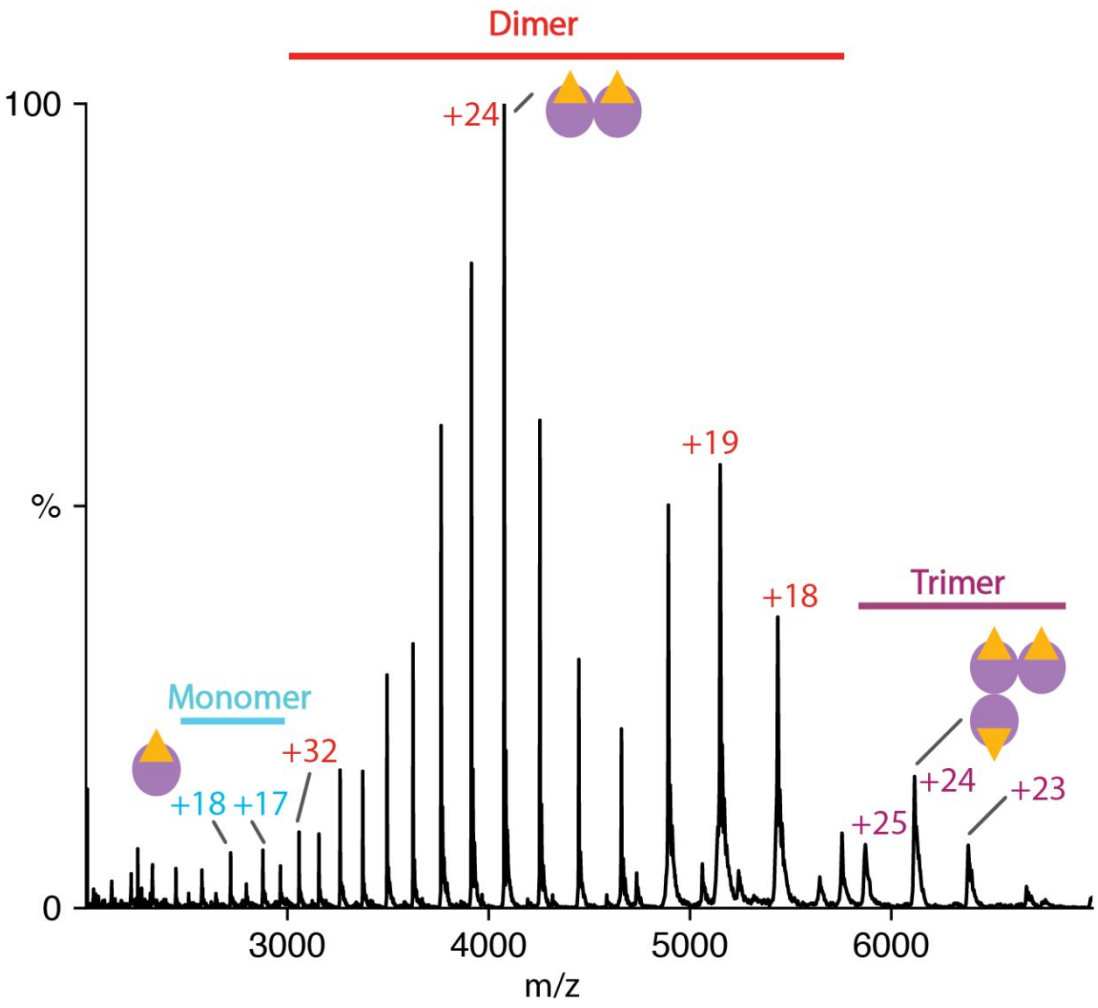

Figure S7. Mass spectrum of ICL1 under denaturing conditions at increased activating energy. The mass spectrum is obtained in the presence of 1% formic acid mixed with 5 μM intact *cis*-EpS-treated ICL1. The molecular weights of dissociated monomer, dimer and trimers correspond to binding of one, two and three equivalents of *cis*-EpS, respectively.

SUPPLEMENTARY INFORMATION

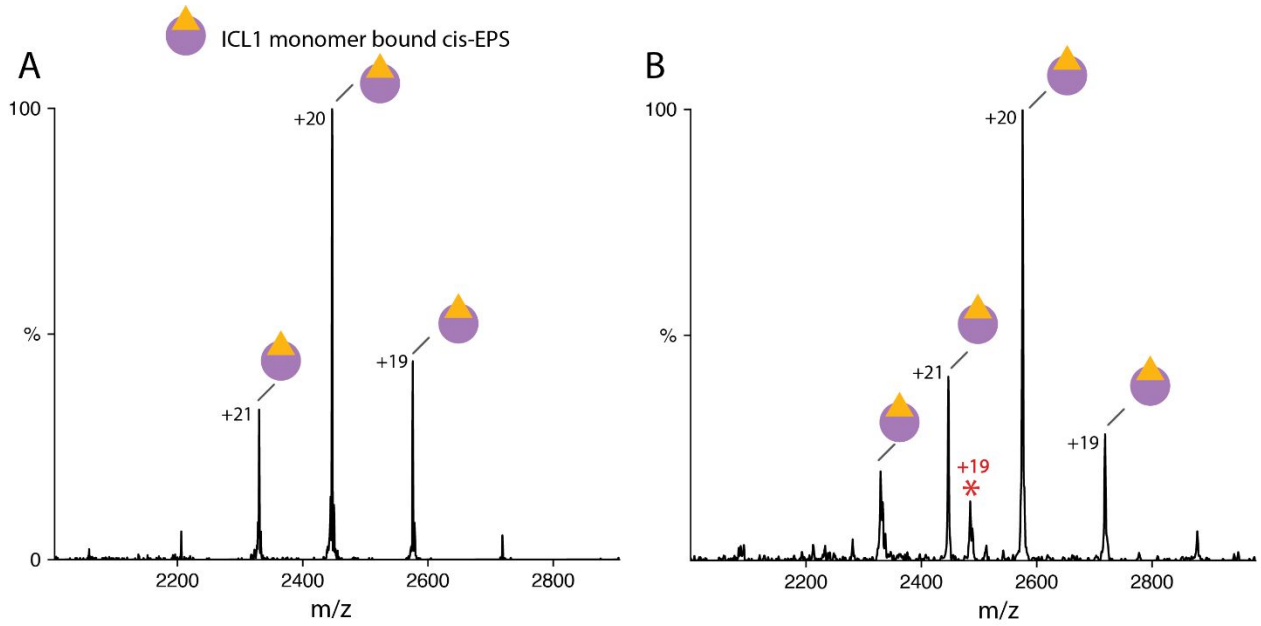

Figure S8. The mass spectra shown for *cis*-EPS bound ICL1 monomer (A) treated in the presence of 1 mM glycolate, and (B) treated in the presence of 1 mM glycolate after a four-day incubation at 4 ^{0}C. The star indicates a truncated monomer with a measured mass of 47190 Da.

SUPPLEMENTARY INFORMATION

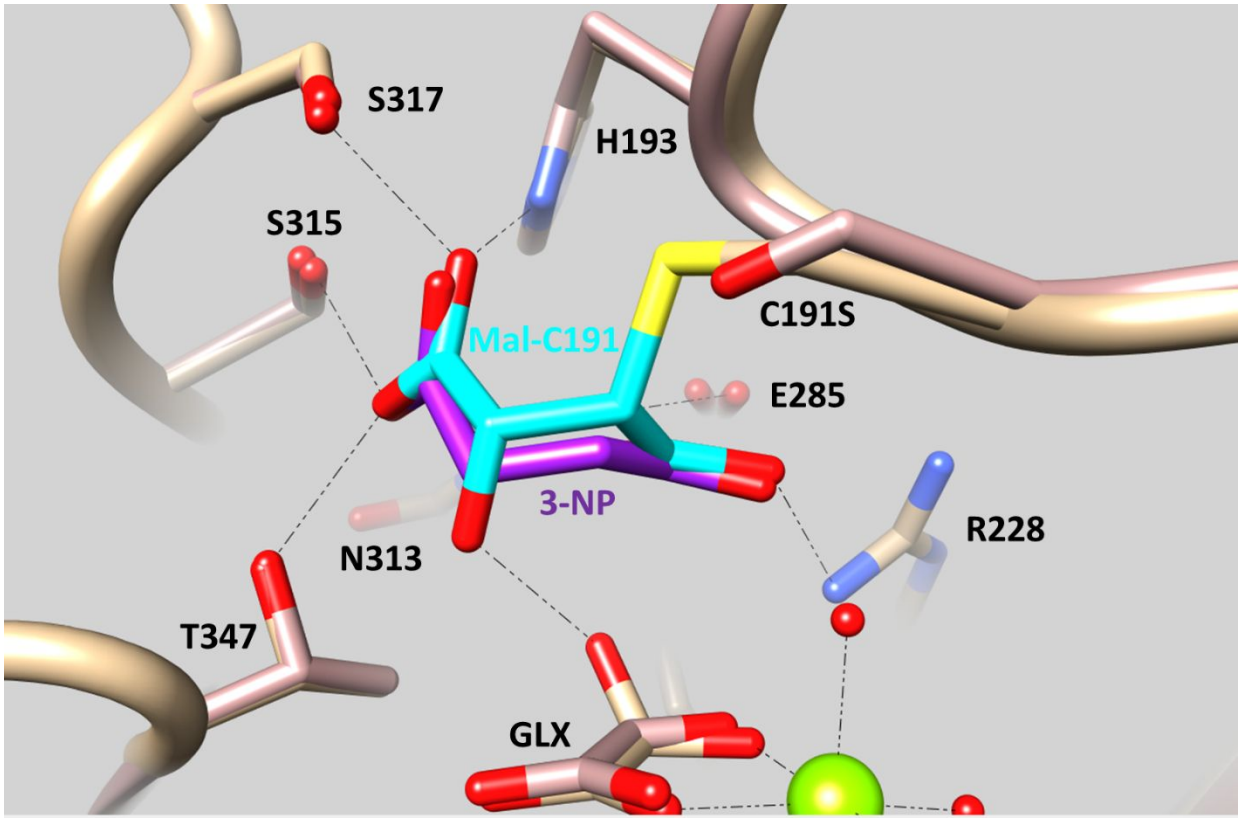

Figure S9. Overlay of ICL1 structures in complex with glyoxylate (gold) and 3-nitropropionate (purple) and (*S*)-3-S malylated (cyan) active site of ICL1. Glyoxylate (Glx) is shown as an aldehyde in ICL1 in its complex with 3-NP, and as its hydrate in the (*S*)-malatyl-Cys191 ICL1 structure. Dashed-lines are potential hydrogen-bonding interactions between the ligands and active-site residues in ICL1.

SUPPLEMENTARY INFORMATION

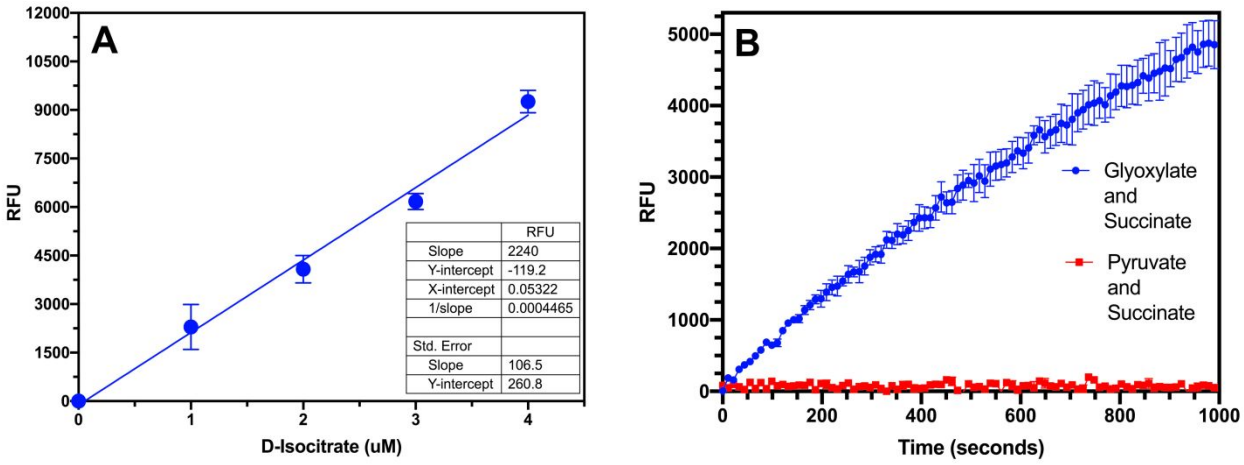

Figure S10. Detection of product D-isocitrate produced from recombinant ICL1 and succinate, as determined by conversion of ICL1-catalysed formation of D-isocitrate detected using a coupled enzyme assay comprised of isocitrate dehydrogenase and diaphorase. **A.** Standard curve of D-isocitrate versus relative fluorescence units (RFUs) when incubated with the coupled assay system. **B.** Incubation of 30 nM ICL1 in the presence of 2 mM glyoxylate and 2 mM succinate or 2 mM pyruvate and 2 mM succinate was analyzed to ensure the assay was specific for the formation of D-isocitrate, and would not detect methyl isocitrate produced from added pyruvate.

SUPPLEMENTARY INFORMATION

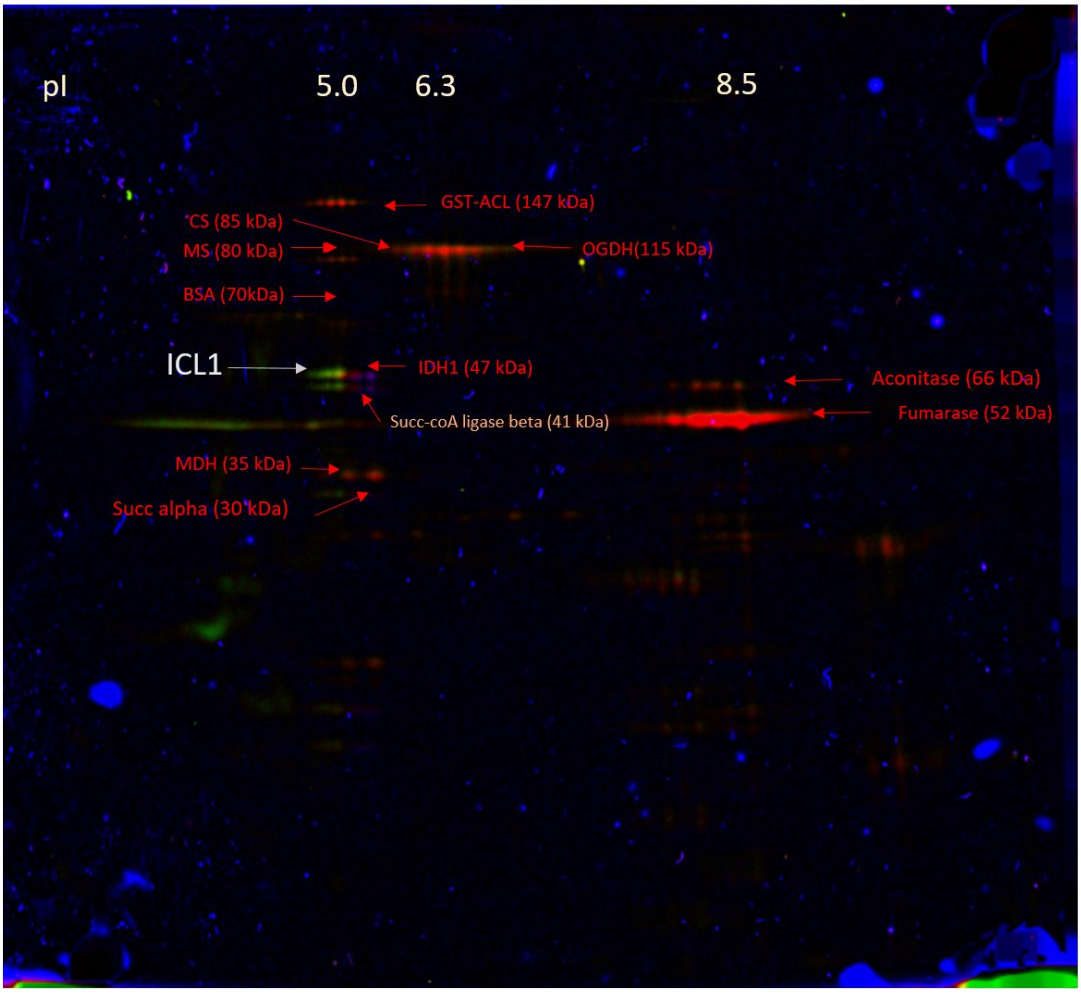

Figure S11. 2-D DIGE analysis of TCA cycle enzymes

A mixture of TCA cycle enzymes (25 µg each) were treated with 1 mM *cis*-EpS for 1 hour, and analyzed in a 2D gel together with a control sample of *cis*-EpS-treated ICL1. Untreated sample and treated sample were labeled with Cy5 and Cy2, respectively. Protein spots shown in red showed no differential migration between untreated and treated samples.

SUPPLEMENTARY INFORMATION

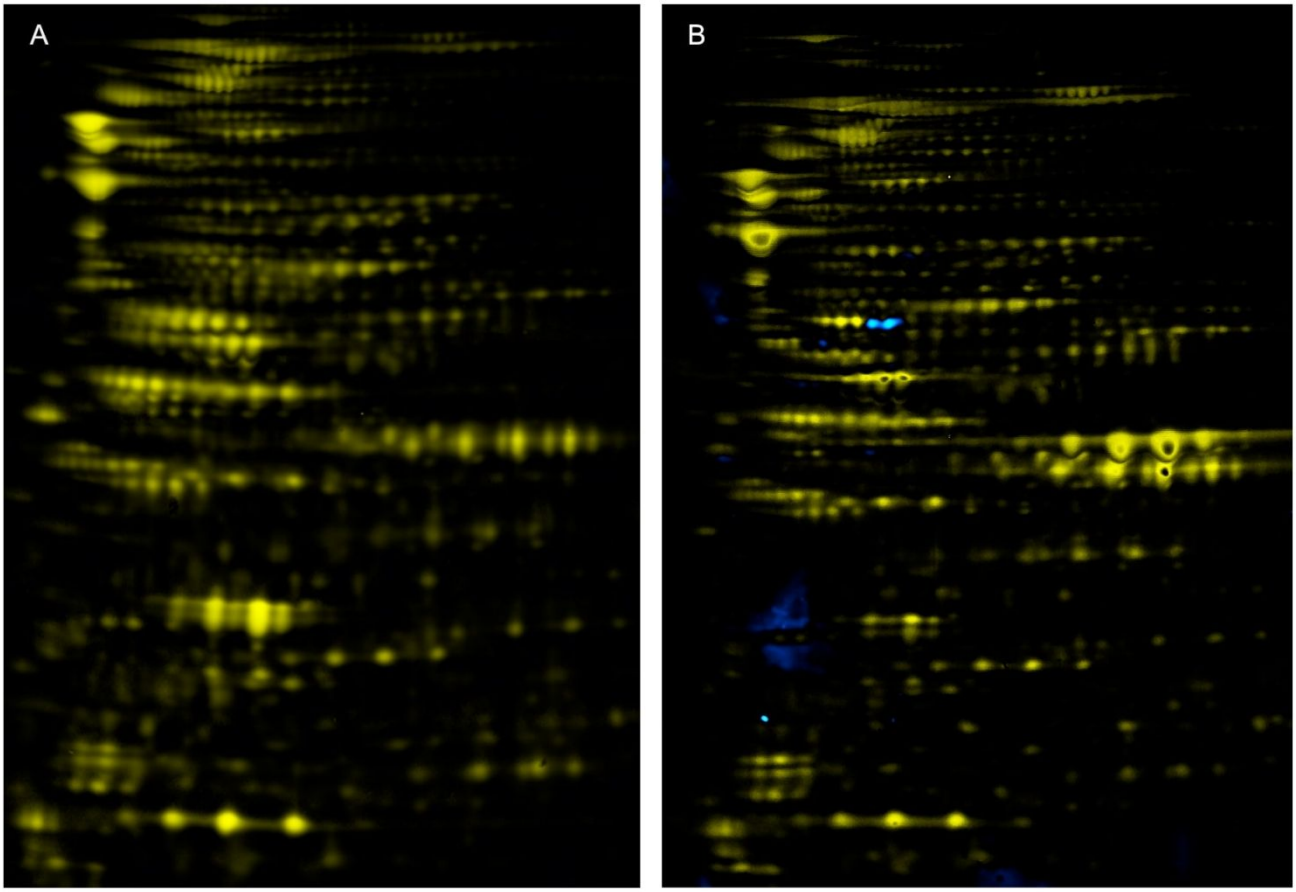

Figure S12. 2D-DIGE of *E.coli* proteome. **A**. Overlay of *E. coli*-transformed with a pUC-19 control vector and either treated with 1 mM *cis*-EpS, followed be labeling with Cy5 dye, or only treated with Cy2 dye. **B**. Overlay of *E.coli* transformed with an *Mtb* ICL1-encoding plasmid, and either treated with 1 mM *cis*-EpS and labeled with Cy5 dye or only labeled with Cy2 dye. Data was processed in ImageJ as described in the methods below.

SUPPLEMENTARY INFORMATION

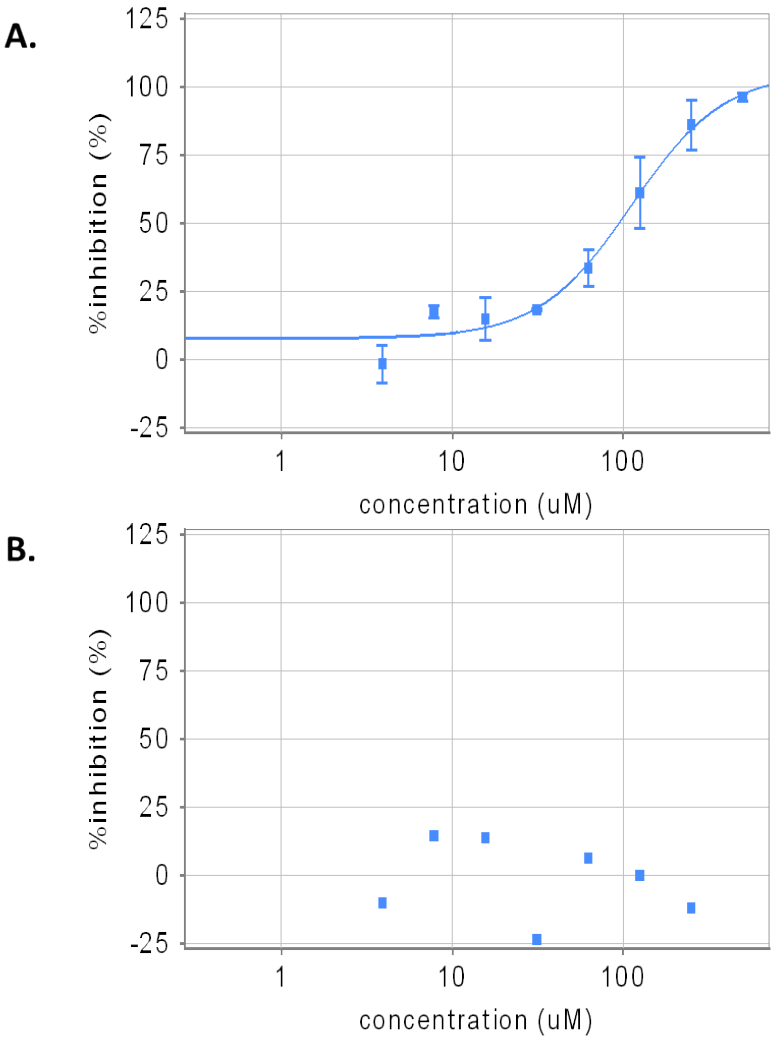

Figure S13 Inhibition of *Mtb mc² 7000* growth by *cis*-EpS and *trans*-EpS.

Effects of (A) *cis*-EpS and (B) *trans*-EpS on *Mtb mc² 7000* grown using acetate as a carbon source. The dose-response curve of c*is*-EpS-induced growth inhibition was fitted to equation $y = 100 - 100/(1+[I]/IC_{50})$ where y is normalized inhibition (%) and [I] is the concentration of *cis*-EpS (x-axis) and IC_{50} represents the concentration of *cis*-EpS that achieves 50% inhibition ($IC_{50} = 100 \pm 10$ µM).

SUPPLEMENTARY INFORMATION

TABLES

Table S1. Inhibition of ICL1 by Substrate Analogs.

Table S1. Inhibition of Isocitrate Lyases 1 by Substrate Analogs.

		M. tuberculosis			*P. indofera** or *N. crassa***		
Analog	Structure	Inhibition Pattern	K_{is} (mM)	K_{ii} (mM)	Inhibition Pattern	K_{is} (mM)	K_{ii} (mM)
(S)-malate	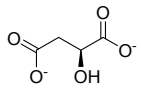	NC	1.4 ± 0.3	7 ± 3	NC	1.3	ND
Glycolate	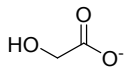	C	0.05 ± 0.01	NA	C	1.5	
(R)-Lactate	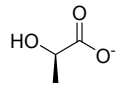	C	1.8 ± 0.7	NA			
Maleate	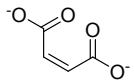	UC	NA	0.30 ± 0.02	NC	ND	0.84
Fumarate	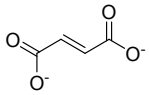	C	1.9 ± 0.4	NA	C	1	NA
Oxaloacetate	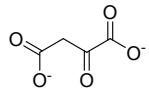	NC	0.14 ± 0.04	0.26 ± 0.02			
Hydroxycitrate	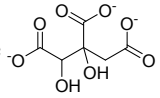	C	8 ± 1 x 10^{-3}	NA			
Cis- aconitate	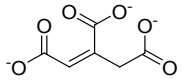	C	0.55 ± 0.08	NA			
Trans -aconitate	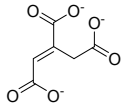	UC	NA	5 ± 1			

[a]Obtained at 37° C, 50 mM HEPES (pH 7.5), 10 mM $MgCl_2$, and 1 mM DTT and 1-100 □M D-isocitrate. C, NC, and UC; competitive, non-competitive (mixed inhibition), and un-competitive inhibition, respectively, in terms of the inhibition pattern vs. variable isocitrate. K_{is}, slope inhibition constant; K_{ii}, intercept inhibition constant. NA,not applicable. ND, no data.

*Johanson, RA, Hill, JM, & McFadden, BA (1974) Isocitrate lyase from Neurospora crassa: Purification, kinetic mechanism and interactions with inhibitors. Biochim, Biophys. Acta 00, 327-340.

**Rao, GR & McFadden, BA (1965) Isocitrate Lyase from Pseudomonas indigofera: IV. specificity and inhibition. Arch. Biochem. Biophys. 112, 294-303.

SUPPLEMENTARY INFORMATION

Table S2. Data collection and refinement statistics for crystallographic analysis of *cis*-EpS-treated ICL1.

	Covalent adduct of cis-2,3-epoxysuccinic acid to ICL1 (6VB9)	Intact cis-2,3-epoxysuccinic acid bound to ICL1 (6WSI)
Data collection		
Space group	$P2_12_12_1$	$P2_12_12_1$
Cell dimensions		
a, *b*, *c* (Å)	75.06,129.06, 167.82	79.17, 134.21, 161.04
α, β, γ (°)	90.00, 90.00, 90.00	90.00, 90.00, 90.00
Resolution (Å)	48.94 – 1.88	71.05 - 1.75
R_{sym} or R_{merge}	0.3 (2.6)	0.1 (1.008)
$I/\sigma I$	2.2 (1.2)	10.1 (1.0)
Completeness (%)	90.7 (53.1)	99.9 (98.6)
Redundancy	9 (4.9)	5.9 (3.3)
Refinement		
Resolution (Å)	48.94 – 1.88	71 – 1.75
No. reflections	119322	172629
$R_{work/}$ R_{free}	0.18 / 0.23	0.16 / 0.196
No. atoms		
Protein	13345	13322
Ligand/ion	103	170
Water	971	1176
B-factors		
Protein	25	22
Ligand/ion	31.5	26
Water	21	24
R.m.s deviations		
Bond lengths (Å)	0.01	0.01
Bond angles (°)	0.85	0.84

*Highest resolution shell is shown in parenthesis.

SUPPLEMENTARY INFORMATION

Table S3. Purified enzymes treated with cis-EpS as evaluated by inhibition/inactivation kinetics and by DIGE isoelectric focusing.

Enzyme	MW	pI	Source	Stock Buffer Conditions
Succinyl CoA synthetase	29.8 kDa (α), 41.4 kDa (β)	6.3 & 5.4	*E. coli*	50 mM HEPES (pH 8.0) 150 mM sodium chloride, 20% glycerol
ATP-citrate lyase (ACL)	147 kDa	6.9	Human	25 mM Tris-HCl (pH 8.0) 100 mM NaCl, 0.05% Tween-20 and 10% glycerol
Citrate Synthase (CS)	85 kDa	6.1 -6.6	Porcine Heart	Water
Malic dehydrogenase (MDH)	36 kDa	6.2	Porcine Heart	2.8 M $(NH_4)_2SO_4$ solution, pH 6.0
Fumarase	50.2 kDa		Human	20 mM Tris-HCl buffer (pH 8.0)
α-ketoglutarate dehydrogenase (α-KGDH)	120 kDa	6.28	Porcine Heart	50% glycerol solution containing ~9 mg/mL bovine serum albumin (BSA), 30% sucrose, 1.5 mM EDTA, 1.5 mM 2-mercaptoethanol, 0.3% Triton™ X-100, 0.003% sodium azide, and 15 mM potassium phosphate, pH 6.8
Aconitase	66 kDa	8.1 -8.5	Porcine Heart	Water
Isocitrate dehydrogenase 1 (IDH1)	47 kDa	6.5	Human	Tris-HCl (pH 8.0), trehalose, ammonium sulfate and DTT
Isocitrate lyase (ICL1)	47.8 kDa	5.3	*M. tuberculosis*	50 mM HEPES (pH7.5) 10 mM MgCl2
Bovine Serum Albumine (BSA)	69 kDa	5.8	*Bos taurus*	see KGDH
Malate synthase (MS)	80 kDa	5	*M. tuberculosis*	50 mM Tris, pH 7.5

SUPPLEMENTARY INFORMATION

Supplementary Methods.

Protein Expression and Purification

A plasmid containing *Mtb icl1* was a gift from Dr. Andrew Murkin of Buffalo University, NY.[1] This construct contains the ICL1 gene (Uniprot: P9WKK6) with an N-terminal, thrombin-cleavable His_6 epitope tag. The recombinant protein was expressed in *E.coli* BL21(DE3) cells, and was expressed and purified as previously described.[1,2] Pure ICL1 was stored in a buffer of 50 mM Tris-HCl (pH 7.0), 150 mM NaCl, and 10% glycerol at –80 °C, or in 25 mM Tris-HCl (pH 7.5), 75 mM NaCl, 0.5 mM DTT and 50% (v/v) glycerol at –20 °C. For mass spectrometry, ICL1 was further purified via gel filtration (HiLoad® 26/600 Superdex® 200 pg, GE Healthcare), in which the column was pre-equilibrated with 50 mM HEPES (pH 7.5) and 150 mM NaCl. Fractions containing the pure tetramer were pooled, concentrated, and stored at -80°C. For crystallography, the His_6 epitope tag was removed by incubation with thrombin, in both the presence and absence of D-isocitrate to protect the tag-free ICL1 from further proteolysis. Truncated ICL2 (Uniprot: Q8VJU4) was expressed and purified as previously described.[2] *E. coli* isocitrate dehydrogenase (ICDH) gene was obtained from an Aska (-) clone containing the *icd* gene in a pCA24N plasmid.[1,3]

Enzyme Assays

Unless otherwise specified, all assays were conducted in clear 96-well plates consisting of 250-µL reaction mixtures containing 50 mM HEPES (pH 7.5), 5 mM $MgCl_2$, and 1 mM DTT at 37ºC. In the direction of isocitrate cleavage, product glyoxylate was reacted with 10 mM phenyl-hydrazine-HCl to form its phenyl-hydrazone product, which was measured spectrophotometrically at A_{324nm} (ε_{324} = 17,000 $M^{-1}cm^{-1}$). In the direction of isocitrate synthesis, product isocitrate was converted to α-ketoglutarate using a coupled-enzyme assay containing 100 nM *E. coli* isocitrate dehydrogenase and 0.25 mM NADP. Absorbance of the product NADPH was measured spectrophotometrically at $A_{340\ nm}$ (ε_{340} = 6,220 $M^{-1}cm^{-1}$). Alternately, isocitrate synthesis was measured using a two-enzyme coupled system containing 0.1 units of bovine isocitrate dehydrogenase (Sigma Aldrich), 0.3 mM $NADP^+$, 0.1 units diaphorase from *Clostridium kluyveri* (Sigma Aldrich) and 50 µM resazurin in the assay buffer described above, but without the addition of 1 mM DTT. The formation of D-isocitrate, concomitant with NADPH formation by isocitrate dehydrogenase, was followed by the conversion of NADPH to $NADP^+$, and resazurin was converted to resorufin by diaphorase catalysis, allowing the detection of resorufin at 525/598 nm (ex/em). This assay was conducted at 25°C in black clear-bottom 96-well half-volume plates (Greiner) with a final reaction volume of 150 µL. All spectrophotometric and fluorescent measurements were recorded on a Biotek® Synergy M2 plate reader equipped with temperature control.

SUPPLEMENTARY INFORMATION

Inhibition Studies.

Analogues of isocitrate, glyoxylate, and succinate were evaluated as inhibitors of ICL1 in reaction mixtures at 37° C, containing 50 mM HEPES (pH 7.5), 10 mM $MgCl_2$, 1 mM DTT and 1-100 μM D-isocitrate. Inhibition patterns apparently conforming to competitive (C), non-competitive or mixed inhibition (NC), and un-competitive (UC) inhibition were fitted to eq S1-S3, respectively, in which

$$v = V_{max}A/(K_a(1 + I/K_{is}) + A) \quad \text{(S1)}$$

$$v = V_{max}A/(K_a(1 + I/K_{is}) + A(1 + I/K_{ii})) \quad \text{(S2)}$$

$$v = V_{max}A/(K_a + A(1 + I/K_{ii})) \quad \text{(S3)}$$

v is initial velocity, V_{max} is maximal velocity, A is the variable or fixed concentration of D-isocitrate, and K_a is the apparent Michaelis constant, I is the changing-fixed concentration of the inhibitor, K_{is} and K_{ii} are the respective slope and intercept inhibition constants. All inhibition data were fitted to eq S2 in order to determine which of the three types of inhibition patterns was best fitted.

Enzyme Inhibition.

For the forward reaction of ICL, residual activity ICL1 (2 nM) was measured in the presence of 0–5 mM *trans*-EpS, 50 or 100 μM (2*R*,3*S*)-isocitrate (D-IC), and glyoxylate formation was quantified as described above. Graphical analysis of inhibition patterns was conducted using Cornish-Bowden plots.[4]

Enzyme Inactivation Studies.

1 μM ICL1 was pre-incubated with variable concentrations of inactivator in reaction mixtures containing 50 mM HEPES (pH 7.5), 5 mM $MgCl_2$, in the presence or absence of 1 mM DTT. Aliquots were withdrawn and diluted 50-fold into reaction mixtures containing 1 mM of D-isocitrate, and glyoxylate formation was measured as described above. Initial rates were normalized to control samples in which no inactivator was added. Also, time courses of ICL inactivation were measured as time-dependent rates of glyoxylate formation as either initial rates (v_i) or slower final rates (v_s). From this, apparent first-order rate constants of ICL inactivation (k_{obs}) were obtained. Experimentally, reaction mixtures (250 μL) contained D-isocitrate (0-200 μM) and *cis*-EpS (0-2.5 μM), to which 2 nM ICL1 was added, and glyoxylate formation was monitored at $OD_{324\ nm}$ for 0-12 min. Likewise, the time-dependent inactivation of 20 nM ICL2 by *cis*-EpS (0-200 μM) was evaluated with D-isocitrate (0-500 μM).

SUPPLEMENTARY INFORMATION

Intrinsic Protein Fluorescence:

ICL1 (1 μM monomers) in 50 mM HEPES and 10 mM $MgCl_2$ (pH 7.5) was combined with either *cis*-EpS (1 μM) or *cis*-EpS (1 μM) and glyoxylate (100 μM). Reaction mixtures (200 μL) were excited at λ_{ex} = 295 nm, and the intrinsic fluorescence emission spectra (λ_{em} = 315–380 nm) was determined at multiple time points (room temperature) using a Biotek Synergy plate reader and black clear-bottom 96-well plates (Greiner). The λ_{max} of ICL1 fluorescence was determined to be 325 nm. All data were corrected by subtracting the background fluorescence observed in a sample of buffer. Upon addition of ligand the spectrum was recorded multiple time points. Each spectrum was normalized, assigning the fluorescent intensity of protein alone at 325 nm to 1. For the samples containing both *cis*-EpS and glyoxylate, we subtracted the glyoxylate spectrum in order to elucidate the relative fluorescent change resulting from *cis*-EpS binding to ICL1. Relative fluorescent change of ICL1 at 325 nm in response to ligand binding were plotted using $F_t = (F_0 - F_{min})*\exp(-k_{obs}*t) + F_{min}$ in which F_t, F_0, and F_{min} are the respective protein fluorescence measured at time t, t=0, respectively, and k_{obs} is the apparent first-order rate constant of diminution of fluorescence.

Double Inhibition of ICL1 by Substrate Analogs.

Double inhibition studies (Yonetani-Theorell analysis[5]), in which the effects of two inhibitors on an enzymatic reaction are evaluated simultaneously to evaluate any synergistic interactions, were conducted for succinate and glyoxylate analogues.[6,7] Initial velocity data were determined at 50 μM D-isocitrate, ICL1 (2 nM), variable concentrations of glycolate (0-0.25 mM) or (*R*)-lactate (0-1 mM) and changing-fixed concentrations of maleate (0 – 0.3 mM), and were plotted as $1/v$ vs. [I], as shown. Data were fitted to both eq S4 and S5 in which K_i and K_j are the apparent inhibition constants for inhibitors I and J, respectively, and α is the interaction factor (indicator of binding synergy) between the two inhibitors.

$$v = V_{max}A/[1 + I/K_i + IJ/(\alpha K_iK_j) + A(1 + J/K_j)] \quad \text{(S4)}$$

$$v = V_{max}A/[1 + I/K_i + J/K_j + IJ/(\alpha K_iK_j) + A(1 + J/K_j)] \quad \text{(S5)}$$

Equation S4 describes the case in which inhibitor I binds solely to free enzyme, and inhibitor J binds to EI and to EA to form EI, EIJ, and EAJ complexes. Equation S5 describes the case in which inhibitor I binds solely to free enzyme, and inhibitor J binds to free enzyme, to EI and to EA, to form EI, EJ, EIJ, and EAJ complexes. Synergistic interactions between inhibitors I and J are provided by the value of α, for which there is synergy when $0 < \alpha < 1$, no binding synergy when $\alpha = 1$, and anti-synergy when $1 < \alpha < \infty$.

SUPPLEMENTARY INFORMATION

Analysis of Inactivation Data. Time courses of enzyme inactivation were fitted to eq S6, a modification of an equation for fitting time-dependent inhibition wherein the final steady-state rate is zero, due to apparent irreversible inactivation.[8] [P] is the concentration of glyoxylate, v_i is the initial rate (mOD/s) or ([Glx]/s), t is the time of reaction, and k_{obs} is the apparent first-order rate constant of inactivation obtained at each concentration of inactivator. Values of k_{obs} (the maximal observed rate constant (s^{-1})) were re-plotted using eq. S7, wherein [I] is the concentration of inactivator, k_{inact} is the maximal rate constant of inactivation, and K_{inact}' is the mechanism-dependent, apparent concentration of inactivator at which the observed rate constant of inactivation is half that of k_{inact}.

$$[P] = \frac{v_i\left(1 - e^{-k_{obs}t}\right)}{k_{obs}} \qquad \text{(S6)}$$

$$k_{obs} = (k_{inact}[I])/(K_{inact}(1 + K_a/[A]) + [I]) \qquad \text{(S7)}$$

Apparent values of $k_{obs'}$ vs. [isocitrate] or [succinate] as shown in Fig. 1c were respectively fitted to eq S8 and S9, and K_{inact}' at variable concentrations of D-isocitrate or succinate [A], wherein K_a are the Michaelis constants of the two substrates, were fitted to eqs S8 and S9 for uncompetitive and competitive inactivators, respectively.

$$k_{obs'} = k_{obs}\left(1 + \frac{K_a}{[A]}\right) \qquad \text{(S8)}$$

$$k_{obs'} = k_{obs}\left(1 + \frac{[A]}{K_a}\right) \qquad \text{(S9)}$$

$$K_{inact'} = K_{inact}\left(1 + \frac{K_a}{[A]}\right) \qquad \text{(S10a)}$$

$$k_{inact'} = k_{inact}\left(1 + \frac{K_a}{[A]}\right) \qquad \text{(S10b)}$$

Data of [glyoxylate] vs. time at changing-fixed concentrations of *cis*-EpS were also fitted globally, that is, all concentrations of the inactivator simultaneously, to eq. 5, for which K_{i1} is the inhibition constant for binding of I to E-Glx, and k_{inact} and K_{inact} are limiting values as defined below.

SUPPLEMENTARY INFORMATION

$$[P] = \left[\frac{\frac{k_{cat}[E_t][A]}{\left(Ka + [A]\left(1 + \frac{[I]}{K_{i1}}\right)\right)}}{\left(\frac{k_{inact}[I]}{K_{inact}\left(1 + \frac{K_a}{[A]}\right) + [I]}\right)}\right]\left[1 - \exp\left(\frac{-tk_{inact}[I]}{K_{inact}\left(1 + \frac{K_a}{[A]}\right) + [I]}\right)\right] \quad \text{(S11)}$$

Crystallographic Analysis of cis-EpS-treated ICL1.

The data were indexed, integrated, and scaled using HKL2000[9] for the covalent adduct structure (6VB9), and by XDS, Pointless and Aimless - for the intact *cis*-EpS complex structure (6WSI)[9] The structures were solved by molecular replacement with MOLREP[10] using the ICL1 structure of PDB 1F8I as a model[11]. The refinement was done in PHENIX[12] including a simulated annealing routine on the first few rounds. Strong and clear electron density was observed for the covalent adduct on Cys_{191} in all four protein chains of the asymmetric unit for the 6VB9. Proposed modification resulting from the attack of the cysteine on the epoxide concurrent with ring opening fitted the extra density perfectly, and was refined into it as S-malyl-Cys_{191}, with alternating rounds of manual building and correction using COOT[13] with phenix.refine. Interestingly, the magnesium ion appeared to be coordinated by glyoxylate-hydrate in 6VB9 structure, while just glyoxylate refined better in 6WSI. Although no glyoxylate was added in crystallization, the protein was exposed to isocitrate during purification in the case of 6VB9, at the step of the affinity tag cleavage, which upon turnover resulted in residual glyoxylate in the observed crystal. 6WSI structure was obtained with no exogenous glyoxylate added. The analysis of recombinant purified ICL1 sample by mass spectrometry showed that it co-purifies with glyoxylate, which was also verified enzymatically. Hence we built glyoxylate in the 6WSI structure.

Selectivity Analysis of cis-EpS with Enzymes of the Tri-Carboxylic Acid Cycle and Others.

A list of enzymes that were tested for analysis of the selectivity of *cis*-EpS is included in Table S3. Studies of the inhibition or inactivation of these enzymes was carried out at fixed concentrations of substrates, approximately at values of $2K_M$, and in the presence of 1 mM *cis*-EpS, and time-course data were collected for 0-20 min. A control sample containing no *cis*-EpS was included for each enzyme tested. Enzyme activity of succinyl-CoA synthetase was detected via a pyruvate kinase/lactate dehydrogenase-coupling assay. Malate dehydrogenase and citrate synthase activities were measured by following the formation of oxaloacetate upon its reaction with phenylhydrazine, via spectrophotometric measurement of the increase in absorbance at 324 nm. Similarly, phenylhydrazine was used to determine activity of 2-oxoglutarate dehydrogenase (α-keto-glutarate dehydrogenase) by detection of the 2-oxoglutarate phenylhydrazone product formation at A_{324}. For fumarase, formation of malate was coupled with malate dehydrogenase and phenylhydrazine assay in which oxaloacetate phenylhydrazone and NADH formation were measured concurrently (A_{324} and A_{340}, respectively).

SUPPLEMENTARY INFORMATION

Formation of isocitrate from citrate by citrate synthase and ATP-citrate synthase was measured by isocitrate dehydrogenase-coupling assay in which NADPH formation was measured spectrophotometrically at 340 nm.

Inhibition of Mtb Growth on Acetate and Glucose

The effects of *cis*- and *trans*-EpS on cell growth of *M. tuberculosis* was tested as described.[14] The mc^2-7000 strain of *M.* tuberculosis,[15] was grown in 7H9 media with OADC (Middlebrook) supplement, 0.05% Tyloxapol (Sigma) and 25 μg/ml pantothenate to an OD600 of 1-2. Then cells were diluted into testing media to an OD_{600} of 0.01, and pipetted into testing plates, 200 μl per well. The two testing media were: 7H9 media with 0.52% dextrose, 0.085% NaCl, 0.05% Tyloxapol, and 25 μg/ml pantothenate or M9 (Sigma) media with 0.25% Na acetate, 2 mM $MgSO_4$, 0.1 mM $CaCl_2$, 0.05% Tyloxapol, and 25 μg/ml pantothenate. Then each compound was added as a 1/2 serial dilution in DMSO (2% DMSO final in a well). 7H9-dextrose plates were incubated for 6 days before staining with resazurin (Sigma), M9-acetate plates were incubated for 3 weeks, and then for additional 2 days after staining at 37°C. Rifampicin was used as a control: for mc^2-7000 *Mtb* displaying an MIC_{99} of 0.125 μM in 7H9-dextrose, and an MIC_{99} of 0.25 μM in M9-acetate. The normalized percent inhibition for the dose-response plot was calculated using highest rifampicin concentration well reading as a positive control, and 2% DMSO containing well reading as a negative control; each measurement was done in triplicate.

Differential Gel Electrophoresis (DIGE)[16]

E. coli B21 (*DE3*) was transformed with PUC19 (as a control vector) or with a plasmid encoding *Mtb* ICL1 (a gift from Dr. Andrew Murkin of Buffalo University, NY) using electroporation with a Biorad Gene Pulser (200 Ohms, 25 μFd, 1.8kV), and allowed to recover in 0.5-mL of Luria Bactose media with vigorous shaking at 37°C for 45 min. Cell cultures (50-μL) were evenly spread on a LB-agar plate containing 100 μM carbenicillin, and incubated overnight at 37°C. A single colony was picked for growth in a 10-mL overnight culture at 37°C. *E. coli*. Cell pellets were harvested by centrifugation at 6,000g, 4°C. Cell lysates were obtained via physical disruption of cell pellets with a sonicator (50% amplification, 5 seconds on, 15 seconds off until achieving a clear and homogenous cell lysate solution) in a lysis buffer containing 50 mM HEPES (pH 7.5) and 10 mM $MgCl_2$. After sonication, lysates were clarified with centrifugation at 17,000g, 4°C for 10 min, and supernatant was treated with or without 1 mM *cis*-EPS for 1 hr. For commercial preparations of enzymes of the tricarboxylic acid cycle and other enzymes, reaction mixtures containing 2.5 μg of each enzyme were prepared in a buffer containing 50 mM HEPES, 10 mM $MgCl_2$ and 1 mM DTT. Protein samples were then precipitated by the addition of a chloroform/ methanol mixture (1:1), and dissolved in labeling

SUPPLEMENTARY INFORMATION

buffer (7M urea, 2M thiourea, 4% (w/v) CHAPS, 10 mM Tris, pH 8.3). Treated and untreated samples were then labeled with Cy5™ and Cy2™, respectively, on ice and in the dark for 60 min. Lysine (10 mM) was added and incubated for 15 min to quench excess dye. Untreated and treated samples were mixed, and diluted into rehydration solution containing Destreak solution, Bromophenol blue, LB and Pharmalytes to a total volume of 250 µL. The mixture was used to rehydrate 13-cm, pH 3-10NL DryStrips. Isoelectric focusing was performed on a GE Ettan IPGPhor (v2) apparatus at a total of 25,000 volt-hrs. Strips containing proteins were then incubated with DTT (10 mg/ml) and iodoacetamide (25 mg/ml) for 10 min each, prior to loading onto a 12% (SDS) polyacrylamide slab gel. Gels were imaged on a FLA9500 Typhoon imager (GE Health Care) in which blue and green channel images were recorded separately in order to record respective protein spots from Cy2- and Cy5-labeled-samples. Further processing of gel images was carried out with ImageJ software to analyze the differential migration of protein spots in samples which were either treated or un-treated by *cis*-EpS[17,18]. On ImageJ, common protein spots in both channels were obtained by applying the "Min" operator, which retains only mutual pixels in both blue and green channel images. Protein spots found exclusively in untreated or treated samples were obtained from using the "Subtract" operator which reveals pixels shown exclusively in either blue or green channel (see ImageJ software technical note[18]). The resulting images from the "Min" and "Subtract" operators, showing common protein spots, exclusively treated and exclusively untreated protein spots respectively, were then merged into a single 3-color-channel image. Colors of protein spots in figures were applied using the LUT commands and using yellow for treated protein and cyan hot for untreated.

SUPPLEMENTARY INFORMATION

Kinetic Model for Inhibition and Inactivation.

The ordered Uni Bi kinetic mechanism of isocitrate lyase in which succinate is the first product to desorb from the enzyme, and for which a succinate-analogue inhibitor or inactivator (I) may bind to either free enzyme E or the E-glyoxylate complex (EQ) complex is described by the model below where A = isocitrate, P = succinate, Q = glyoxylate, and I is an inhibitor or inactivator that binds to E or EQ (E-glyoxylate). The EI and EQI may then progress to the respective complexes EI* and EQI*, and in the case in which irreversible inactivation occurs, $k_{12} = k_{16} = 0$. The derivation below for time-dependent inactivation of ICL1 by *cis*-EpS is provided because this has not been published for an inactivator that binds as a product analogue.

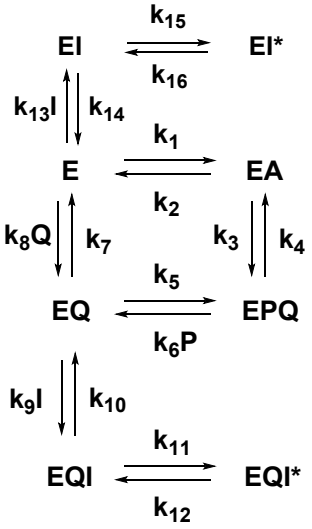

Solution of the steady-state initial rate (v) by King-Altman analysis results in the enzyme distribution equations below, and the rate law of eq (1).

$$E/E_t = (k_2k_4k_7 + k_2k_5k_7 + k_2k_4k_6P + k_3k_5k_7)k_{10}k_{12}k_{14}k_{16} / E_t$$

SUPPLEMENTARY INFORMATION

$EA/E_t = (k_1k_4k_7A + k_1k_5k_7A + k_1k_4k_6AP + k_4k_6k_8PQ)\, k_{10}k_{12}k_{14}k_{16} / E_t$

$EPQ/E_t = (k_1k_3k_7A + k_2k_6k_8PQ + k_1k_3k_6AP + k_3k_6k_8PQ)\, k_{10}k_{12}k_{14}k_{16} / E_t$

$EQ/E_t = (k_2k_4k_8Q + k_2k_5k_8Q + k_1k_3k_5A + k_3k_5k_8Q)\, k_{10}k_{12}k_{14}k_{16} / E_t$

$EQI/E_t = (k_2k_4k_8QI + k_2k_5k_8QI + k_1k_3k_5AI + k_3k_5k_8QI)k_9k_{12}k_{14}k_{16} / E_t$

$EQI^*/E_t = (k_2k_4k_8QI + k_2k_5k_8QI + k_1k_3k_5AI + k_3k_5k_8QI)k_9k_{11}k_{14}k_{16} / E_t$

$EI/E_t = (k_2k_4k_7 + k_2k_5k_7 + k_2k_4k_6P + k_3k_5k_7)k_{10}k_{12}k_{13}k_{16}I / E_t$

$EI^*/E_t = (k_2k_4k_7 + k_2k_5k_7 + k_2k_4k_6P + k_3k_5k_7)k_{10}k_{12}k_{13}k_{15}I / E_t$

$$v = k_1A(E/E_t) - k_2(EA/E_t) \quad (1)$$

Under initial velocity conditions, $P = Q = 0$

And so:

$$E_t = [(k_2k_4k_7 + k_2k_5k_7 + k_3k_5k_7)k_{10}k_{12}(k_{14}k_{16} + k_{13}k_{15}I + k_{13}k_{16}I) + (k_1k_4k_7A + k_1k_5k_7A)k_{10}k_{12}k_{14}k_{16} \quad (2)$$

$$+ (k_1k_3k_7A)k_{10}k_{12}k_{14}k_{16} + (k_1k_3k_5A)k_{10}k_{12} + (k_1k_3k_5AI)k_9k_{12}k_{14}k_{16} + (k_1k_3k_5AI)k_9k_{11}k_{14}k_{16}]$$

$$E_t = k_{10}k_{12}k_{14}k_{16}[(k_2k_4 + k_2k_5 + k_3k_5)k_7)(1 + I/K_{is1}K_{is}^* + I/K_{is1}) + k_1((k_4 + k_5)k_7 + k_3(k_5 + k_7))A + \quad (3)$$

$$k_1k_3k_5A(I/K_{ii})(1 + 1/K_{ii}^*)]$$

The initial velocity expression is then:

$$v = k_1k_3k_5k_7A/[(k_2k_4 + k_2k_5 + k_3k_5)k_7)(1 + I/K_{is1}K_{is}^* + I/K_{is1}) + k_1A((k_4 + k_5)k_7 + k_3(k_5 + k_7)) + \quad (4)$$

$$k_1k_3k_5A(I/K_{ii})(1 + 1/K_{ii}^*)]$$

SUPPLEMENTARY INFORMATION

$k_{cat} = k_3k_5k_7/(k_4 + k_5)k_7 + k_3(k_5 + k_7)$

$K_a = [(k_2(k_4 + k_5) + k_3k_5)k_7 / (k_1[(k_4 + k_5)k_7 + k_3(k_5 + k_7)]$

Where, for an irreversible inactivator I:

$K_{is1} = K_{i1} = k_{14}/k_{13}$

$K_{is*} = K_{i1*} = k_{16}/k_{15} = 0$

$1/K_{ii} = k_3k_5/((k_4 + k_5)k_7 + k_3(k_5 + k_7))K_{i2} = k_{cat}/k_7K_{i2}$

$K_{ii} = K_{i2}k_7/k_{cat} = (k_{10}/k_9)(k_7/k_{cat})$

$K_{i2} = k_{10}/k_9$

$K_{i2*} = k_{12}/k_{11} = 0$

Note: $K_{ii}/K_{i2} = k_7/k_{cat}$ where $K_{i2} = K_{is2}$ is for a competitive inhibitor in the reverse reaction direction.

This results in eq 5, which describes the formation of both the tight-binding or irreversible covalent complexes of EI* and EQI*:

$$v = k_{cat}E_tA/[K_a(1 + I/K_{is1}K_{i1}* + I/K_{is1}) + A(1 + I/(K_{ii}(1 + K_{i2}*)] \quad (5)$$

Note: $1/K_{ii}(1 + K_{i2}*) = k_{cat}/(k_7k_{10}/k_9)(1 + k_{12}/k_{11}) = k_{cat}/(k_7k_{10}/k_9)((k_{11} + k_{12})/k_{11})$ (6)

$= [(k_{12} + k_{11})]/ (k_{cat}/k_7)(k_{10}k_{12})/(k_9)]$

The reciprocal of this is: $(k_{cat}k_9/k_7k_{10}k_{12})/ (k_{12} + k_{11})$

$$(k_{cat}/k_7)(k_{10}/k_9)(k_{12}/(k_{12} + k_{11})) = K_{ii}K_{i2}* \quad (7)$$

$$\text{So: } v = k_{cat}E_tA/[K_a(1 + I/K_{is1}K_{is}* + I/K_{is1}) + A(1 + I/K_{ii} + I/K_{ii}K_{i2}*))] \quad (8)$$

SUPPLEMENTARY INFORMATION

As EI and EQI complexes progress over time to the tighter-binding EI* and EQI* complexes, the initial steady-state rate v_i (eq 9) becomes the slower steady-state rate v_s described by eq 10.

$$v_i = k_{cat}E_tA/[K_a(1 + I/K_{is1}) + A(1 + I/K_{ii})] \quad (9)$$

$$v_s = k_{cat}E_tA/[K_a(1 + I/K_{is1}K_{is}* + I/K_{is1}) + A(1 + I/K_{ii} + I/K_{ii}K_{i2}*))] \quad (10)$$

Case 1: The EQI complex forms but not EI:

From the scheme above, under steady-state conditions:

$$E_t = E + EA + EQI \quad (11)$$

$$K_a = [E][A]/[EA] = ([E][A]/[EA])([EA]/[EPQ])([EPQ)/(EQ)] = [E][A]/[EQ] \quad (12)$$

$$[E] = (K_a/[A])[EQ]$$

$$[EQ]/([E] + [EQ]) = [EQ]/([EQ] + [EQ]K_a/[A]) = 1/(1 + K_a/[A]) \quad (13)$$

$$k_{9''}[EQ]/([E] + [EQ]) = k_9k_{11}[I]/[(k_{10} + k_{11})(1 + K_a/[A])] \quad (14a)$$

which describes uncompetitive inactivation; and for competitive inhibition:

$$k_{9''}[EQ]/([E] + [EQ]) = k_9k_{11}[I]/[(k_{10} + k_{11})(1 + [A]/K_a)] \quad (14b)$$

Case 2: The case where I binds to E and EQ but only EQI goes on to form EQI*:

$$E_t = E + EA + EI + EQI = E + EQ + EI + EQI$$

$$K_a = [E][A]/[EA] = ([E][A]/[EA])([EA]/[EPQ])([EPQ)/(EQ)] = [E][A]/[EQ]$$

$$[E] = (K_a/[A])[EQ]$$

SUPPLEMENTARY INFORMATION

$[EI] = [E][I]/K_{i1} = [EQ](K_a/[A][I]/K_{i1}) = [EQ][I]K_a/[A]K_{i1}$

$E_t = E + EQ + EI = EQ(1 + (K_a/[A]) + [I]K_a/[A]K_{i1})$

$k_{9'} = k_9EQ/(E + EI + EQ) = k_9k_{11}[I]/[(k_{10} + k_{11})(1 + (K_a/[A])(1 + I/K_{i1})]$ (15)

Derivation of the time-course equations for Cases 1 and 2, in which $k_9' = k_9/(1 + K_a/[A])$ and $k_9/(1 + (K_a/[A])(1 + I/K_{i1})]$, respectively :

$d[EQ]/dt = k_{9'}[EQ][I] - k_{10}[EQI]$ (16)

$d[EQI]/dt = k_{9'}[EQ][I] + k_{12}[EQI^*] - (k_{10} + k_{11})[EQI]$ (17)

$d[EQI^*]/dt = k_{11}[EQI] - k_{12}[EQI^*]$ (18)

Re-differentiation of eq 18 gives eq 19.

$d^2[EQI^*]/dt^2 = k_{11}d[EQI]/dt - k_{12}d[EQI^*]/dt$ (19)

Substitution of eq 17 leads to:

$d^2[EQI^*]/dt^2 = k_{11}[k_{9'}[EQ] + k_{12}[EQI^*] - (k_{10} + k_{11})[EQI]] - k_{12}d[EQI^*]/dt$ (20)

$[EQ] = E_t - ([EQI] + [EQI^*])$ (21)

Substitution of eq 21 gives:

$d^2[EQI^*]/dt^2 = k_{11}[k_{9'}[I]E_t - ([EQI] + [EQI^*]) + k_{12}[EQI^*] - (k_{10} + k_{11})[EQI]] - k_{12}d[EQI^*]/dt$ (22)

$d^2[EQI^*]/dt^2 =$

$k_{9'}k_{11}[I]E_t - k_{11}[EQI]\{k_{9'}[I] + k_{10} + k_{11}) + k_{9'}k_{11}[I][EQI^*]\} + k_{11}k_{12}[EQI^*] - k_{12}d[EQI^*]/dt$ (23)

$d^2[EQI^*]/dt^2 + k_{12}d[EQI^*]/dt = k_{9'}k_{11}[I]E_t - \{k_{11}[EQI](k_{9'}[I] + k_{10} + k_{11}) + k_{9'}k_{11}[I][EQI^*]\}$ (24)

SUPPLEMENTARY INFORMATION

$+ k_{11}k_{12}[EQI^*]$

$$d^2[EQI^*]/dt^2 + k_{12}d[EQI^*]/dt = k_{9'}k_{11}[I]E_t - k_{11}[EQI]((k_{9'}[I] + k_{10} + k_{11} + k_{9'}k_{11}[I][EQI^*]\} \quad (25)$$

$+ k_{11}k_{12}[EQI^*]$

$$(1/k_{11})d[EQI^*]/dt + (k_{12}/k_{11})[EQI^*] = [EQI] \quad (26)$$

Substitution of eq 26 for [EQI] in eq 25 gives eq 27:

$$d^2[EQI^*]/dt^2 + k_{12}d[EQI^*]/dt = k_{9'}k_{11}[I]E_t - k_{11}[(1/k_{11})d[EQI^*]/dt$$

$$+ (k_{12}/k_{11})[EQI^*])[k_{9'}[I] + k_{10} + k_{11})] - k_{9'}k_{11}[I][EQI^*] + k_{11}k_{12}[EQI^*] \quad (27)$$

$$d^2[EQI^*]/dt^2 + [k_{9'}[I] + k_{10} + k_{11} + k_{12}]d[EQI^*]/dt + [EQI^*]\{(k_{12})(k_{9'}[I] + k_{10})]$$

$$+ k_{9'}k_{11}[I]\} - k_{9'}k_{11}[I]E_t = 0 \quad (28)$$

Solutions to eq 28 include:

$$\lambda_{1,2} = -(k_{9'}I + k_{10} + k_{11} + k_{12})/2 \pm [(k_{9'}I + k_{10} + k_{11} + k_{12})^2 - 4(k_{9'}k_{11}I + k_{12}(k_{9'}I + k_{10})]^{1/2}/2 \quad (29)$$

$$\lambda_1 = (½)(a + q) \quad (30)$$

$$\lambda_2 = (½)(a - q) \quad (31)$$

SUPPLEMENTARY INFORMATION

$$a = (k_9 \cdot I + k_{10} + k_{11} + k_{12}) \quad (32)$$

$$q = [a^2 - 4((k_9 \cdot k_{11} I + k_{12}(k_9 \cdot I + k_{10})]]^{1/2} \quad (33)$$

$$\lambda_1 + \lambda_2 = (½)(a + q) + (½)(a - q) = (½)2a = a \quad (34)$$

And as $\lambda_1 >> \lambda_2$

$$\lambda_1\lambda_2 = (½)(a - q) = ¼([a^2 - (a^2 - 4(k_9 \cdot k_{11} I + k_{12}(k_9 \cdot I + k_{10})] = k_9 \cdot k_{11} I + k_{12}(k_9 \cdot I + k_{10}) \quad (35)$$

$$\lambda_1\lambda_2/(\lambda_1 + \lambda_2) = \lambda_1\lambda_2/(\lambda_1) = \lambda_2 = (k_9 \cdot k_{11} I + k_{12}(k_9 \cdot I + k_{10})) / (k_9 \cdot I + k_{10} + k_{11} + k_{12}) \quad (36)$$

$$(EQI^*)_t = A_0(1 + (\lambda_2/(\lambda_1 - \lambda_2))e^{\lambda_1 t} - (\lambda_1/(\lambda_1 - \lambda_2))e^{\lambda_2 t}) \quad (37)$$

$$A_0 = k_9 \cdot k_{11} I E_t/\lambda_1\lambda_2 = k_9 \cdot k_{11} I E_t /(k_9 \cdot k_{11} I + k_{12}(k_9 \cdot I + k_{10})) \quad (38)$$

$$k_{obs} = (k_9 \cdot k_{11} I/(k_9 \cdot I + k_{10})) + k_{12})/$$

$$(1 + (k_{11} + k_{12})/ (k_9 \cdot I + k_{10})) \quad (39)$$

$$k_{obs} = (k_9 \cdot k_{11} I + k_{12}(k_9 \cdot I + k_{10})) / (k_9 \cdot I + k_{10} + k_{11} + k_{12})$$

$$k_{obs} = (k_9 \cdot k_{11} I + \cancel{k_{12}(k_9 \cdot I + k_{10})}) / (k_9 \cdot I + k_{10} + k_{11} + \cancel{k_{12}})$$

$$k_{obs} = k_{11} I / (I + (k_{10} + k_{11})/k_9') $$

And for an irreversible inactivator, $k_{12} = 0$, and so eq 39 becomes:

$$k_{obs} = k_9 \cdot k_{11} I / (k_9 \cdot I + k_{10} + k_{11}) = k_{11} I / (I + (k_{10} + k_{11})/k_9') $$

Case 1: $k_{obs} = k_{11} I /[I + (k_{10} + k_{11})(1 + K_a/[A])/k_9]$ (40)

SUPPLEMENTARY INFORMATION

Case 2: $k_{obs} = k_{11}I /[I + (k_{10} + k_{11})(1 + (K_a/[A])(1 + [I]/K_{i1})/k_9]$ (41)

Where we may define:

$K_{inact} = (k_{10} + k_{11})/k_9$ and $k_{inact} = k_{11}$ (42)

From Sungman Cha (1974), the rate of product formation in the presence of a time-dependent inhibitor or inactivator is given by eq (43):

$d[P]/dt = v = v_s + (v_s - v_i)e^{-kobs*t}$ (43)

$d[P] = v_s\, dt + (v_s - v_i)e^{-kobs*t}\, dt$

$\int d[P] = v_s \int dt + (v_s - v_i) \int e^{-kobs*t}\, dt$

$[P] = v_s t + ((v_i - v_s)/k_{obs})(1 - e^{-kobs*t})$ (44)

For irreversible inactivators, $v_s = 0$, and eq 44 becomes eq 45:

$[P] = ((v_i)/k_{obs})(1 - e^{-kobs*t})$ (45)

For an uncompetitive inactivator and Case 1, eq 45 becomes eq 46:

$[P] = [k_{cat}E_tA/(K_a(1 + I/K_{is1}) + A(1 + I/K_{ii}))][k_{inact}I /[I + K_{inact}(1 + K_a/[A])] *$ (46)

$[1 – \exp (-tk_{inact}I /(I + K_{inact}(1 + K_a/[A])]$

SUPPLEMENTARY INFORMATION

References:

1. Moynihan MM & Murkin AS (2014) Cysteine is the general base that serves in catalysis by isocitrate lyase and in mechanism-based inhibition by 3-nitropropionate. *Biochemistry* 53(1):178-187.
2. Pham TV*, et al.* (2017) Mechanism-based inactivator of isocitrate lyases 1 and 2 from *Mycobacterium tuberculosis*. *Proceedings of the National Academy of Sciences of the United States of America* 114(29):7617-7622.
3. Kitagawa M*, et al.* (2005) Complete set of ORF clones of *Escherichia coli* ASKA library (A Complete S et of E. coli K -12 ORF A rchive): Unique Resources for Biological Research. *DNA Research* 12(5):291-299.
4. Cornish-Bowden A (1974) A simple graphical method for determining the inhibition constants of mixed, uncompetitive and non-competitive inhibitors. *Biochem J* 137(1):143-144.
5. Yonetani T (1982) [26] The Yonetani-Theorell graphical method for examining overlapping subsites of enzyme active centers. *Methods in Enzymology*, ed Daniel LP (Academic Press), Vol Volume 87, pp 500-509.
6. Asante-Appiah E & Chan WW (1996) Analysis of the interactions between an enzyme and multiple inhibitors using combination plots. *The Biochemical journal* 320 (Pt 1)(Pt 1):17-26.
7. Yonetani T & Theorell H (1964) Studies on liver alcohol hydrogenase complexes. 3. Multiple inhibition kinetics in the presence of two competitive inhibitors. *Archives of biochemistry and biophysics* 106:243-251.
8. Morrison JF & Walsh CT (2006) The Behavior and Significance of Slow-Binding Enzyme Inhibitors. *Advances in Enzymology and Related Areas of Molecular Biology* 61:101.
9. Otwinowski Z & Minor W (1997) [20] Processing of X-ray diffraction data collected in oscillation mode. *Methods in Enzymology*, (Academic Press), Vol 276, pp 307-326.
10. Vagin A & Teplyakov A (2009) Molecular replacement with MOLREP. *Acta Crystallographica Section D* 66(1):22--25.
11. Sharma V*, et al.* (2000) Structure of isocitrate lyase, a persistence factor of *Mycobacterium tuberculosis*. *Nat Struct Mol Biol* 7(8):663-668.
12. Adams PD*, et al.* (2010) PHENIX: a comprehensive Python-based system for macromolecular structure solution. *Acta Crystallogr D Biol Crystallogr* 66(Pt 2):213-221.
13. Emsley P, Lohkamp B, Scott WG, & Cowtan K (2010) Features and development of Coot. *Acta Crystallogr D Biol Crystallogr* 66(Pt 4):486-501.
14. Krieger Inna V*, et al.* (2015) Structure-Guided Discovery of Phenyl-diketo Acids as Potent Inhibitors of *M. tuberculosis* Malate Synthase. *Chem. & Biol.* 19(12):1556-1567.

SUPPLEMENTARY INFORMATION

15. Sambandamurthy VK, *et al.* (2006) Mycobacterium tuberculosis ΔRD1 ΔpanCD: A safe and limited replicating mutant strain that protects immunocompetent and immunocompromised mice against experimental tuberculosis. *Vaccine* 24(37):6309-6320.
16. Kondo T & Hirohashi S (2007) Application of highly sensitive fluorescent dyes (CyDye DIGE Fluor saturation dyes) to laser microdissection and two-dimensional difference gel electrophoresis (2D-DIGE) for cancer proteomics. *Nature Protocols* 1:2940.
17. Schneider CA, Rasband WS, & Eliceiri KW (2012) NIH Image to ImageJ: 25 years of image analysis. *Nature Methods* 9(7):671-675.
18. Rueden CT, *et al.* (2017) ImageJ2: ImageJ for the next generation of scientific image data. *J BMC Bioinformatics* 18(1):529.